Science Advances
AAAS

advances.sciencemag.org/cgi/content/full/6/41/eabc6572/DC1

Supplementary Materials for

Solution NMR readily reveals distinct structural folds and interactions in doubly ^{13}C- and ^{19}F-labeled RNAs

Owen B. Becette, Guanghui Zong, Bin Chen, Kehinde M. Taiwo, David A. Case, T. Kwaku Dayie*

*Corresponding author. Email: dayie@umd.edu

Published 7 October 2020, *Sci. Adv.* **6**, eabc6572 (2020)
DOI: 10.1126/sciadv.abc6572

This PDF file includes:

Supplementary Materials and Methods:

RNA in vitro transcription. All RNAs were prepared by in vitro transcription with the following components: 40 mM Tris-HCl (pH 8.3), 1 mM spermidine, 0.01% Triton X-100, 80 mg/mL PEG, 0.3 μM template DNA, 0.3 μM T7 promoter DNA, 25 U thermostable inorganic pyrophosphatase (NEB), and 0.1 mg/mL T7 RNA polymerase. HIV-2 TAR RNAs were synthesized in 10-mL reactions with 5 mM NTPs and 6 mM $MgCl_2$ while hHBV ε RNAs were prepared in 15-mL reactions with 7.5 mM NTPs and 9 mM $MgCl_2$. All RNAs were transcribed and purified as previously described (3,4). Final NMR buffers were as follows: HIV-2 TAR: 10 mM Na_3PO_4 (pH 6.5), 150 mM NaCl, 0.02% NaN_3, 0.1 mM DSS, 100% ^2H_2O; hHBV ε: 10 mM Na_3PO_4 (pH 6.5), 0.02% NaN_3, 0.1 mM DSS, 100% ^2H_2O. Prior to NMR analysis, RNAs were denatured at 95 °C for 2 min then annealed by snap cooling on ice. RNA concentrations were approximated by UV absorbance using extinction coefficients of 387.5 $mM^{-1}cm^{-1}$ for HIV-2 TAR and 768.3 $mM^{-1}cm^{-1}$ for hHBV ε. All RNA concentrations were > 0.5 mM in ~ 300 μL.

Thermal melt analysis. We collected thermal melting profiles for both wildtype (WT) and 5-fluorouridine (5FU) substituted HIV-2 TAR and hHBV ε as previously described (*6, 24*). Briefly, RNAs were diluted to ~ 1 μM in 10 mM sodium cacodylate (pH 6.5) or 10 mM sodium cacodylate (pH 6.5) and 150 mM NaCl, for hHBV ε and HIV-2 TAR, respectively. All RNAs were pre-annealed by heating at 95 °C for 2 min then snap cooled on ice. The absorbance at 260 nm was measured upon heating from 4 to 95 °C with a ramp speed of 1 °C/min and data collection every minute. The thermodynamic parameters for unimolecular folding, ΔH, ΔS, and T_m, were determined by fitting the raw melting profiles to the following equation (*25*):

Equation 1 $$A(T) = A_b^0 + m_b T + \frac{A_t^0 - A_b^0 + (m_t - m_b)T}{1 + e^{\frac{\Delta H}{RT} \frac{\Delta S}{R}}}$$

where $A_{b/t}$ and $m_{b/t}$ are the y-intercept and slope for the bottom/top baseline. We assumed that the RNA's heat capacity did not change upon melting.

Electronic structure calculations. Calculations were carried out on 1-methyl-uracil and 5-fluoro-1-methyl uracil, using geometries optimized at the MP2/ccpVTZ level of theory. Chemical shielding tensors were computed (with GIAO orbitals) at the Hartree-Fock and MP2 levels, as well as with a "pure" density functional (OLYP, (*26*)) and a "hybrid" model (PBE0, (*27*)) that includes 25% of Hartree-Fock exchange. The pcSseg-2 basis, which is optimized for chemical shielding calculations (*28*), was used for calculations of the shielding tensors. To test basis set convergence, the calculations other than MP2 were repeated at the pcSseg-3 basis set level. All calculations used the Gaussian-16 program (*29*).

The symmetric part of the shielding tensor was diagonalized to obtain principal shielding components; principal components for a traceless shift tensor are reported as $\delta_{11} = \sigma_{iso} - \sigma_{11}$, etc., where σ_{iso} is one-third the trace of the shielding tensor. Shift tensors are ordered such that δ_{11} is the least shielded, and δ_{33} is the most shielded component.

A summary of the results is shown in Tables S2 and S3. In each case, the rows are ordered by decreasing amount of Hartree Fock exchange, from 100% (HF) to 25% (PBE0) to 0% (PBE or OLYP). There is no comparable fraction for the MP2 results. For both molecules, the overall anisotropy Δ for ^{13}C5 becomes smaller (closer to zero) as the amount of Hartree-Fock exchange decreases. Results for MP2 are generally closest to the pure functional OLYP results. Increasing the basis set size from pcSseg-2 to pcSseg-3 has very little effect. Results for the ^{19}F5 tensor are more varied. Here Δ becomes larger (more negative) as the amount of Hartree-Fock exchange decreases, and the MP2 results are closest to PBE0 rather than OLYP.

If one excludes the Hartree-Fock calculations, the shift anisotropies vary by about 15% over the range of DFT and MP2 calculations studied. Further studies are ongoing to examine the effects of using the 1-methyl base analogue (rather than a ribose at the N1 position), and the effects of incorporating uracil or its fluorine analogue into the RNA helix. For the purposes of the illustrative relaxation calculations reported here, we chose to insert the OLYP/pcSseg-2 tensors into the Spinach spin simulation program (*30*). Studies of the sensitivity of relaxation results to assumptions about CSA tensors and their orientations will be reported elsewhere.

Solution NMR spectroscopy. All ^{1}H/^{19}F-^{13}C TROSY spectra were collected at 298 K using a Bruker 600 MHz Avance III spectrometer equipped with a BBI and TXI probe for ^{19}F- and ^{1}H-^{13}C experiments. The ^{19}F-^{13}C TROSY and ^{1}H-^{13}C TROSY experiments were adapted from a sensitivity-and gradient-enhanced ^{1}H-^{15}N TROSY used for proteins (*31,32*). For the ^{19}F-^{13}C TROSY measurements, the carrier was set to -167 and 140 ppm for ^{19}F (ω_2) and ^{13}C (ω_1), respectively. A J-coupling constant of 232 Hz was used for the ^{19}F-^{13}C transfer and 180 Hz coupling was used for the ^{1}H-^{13}C transfer. For the ^{1}H-^{13}C TROSY experiment, the carrier was set to 4.7 ppm and 100.5 ppm for ^{1}H (ω_2) and ^{13}C (ω_1), respectively. 32 transients were collected for each complex point with acquisitions times of 302 ms for ω_2 and 132 ms for ω_1. The interscan delay was set to 2.0 s for both the ^{19}F-^{13}C and ^{1}H-^{13}C TROSY experiments. Total experiment time for measuring each component of the ^{19}F-^{13}C or ^{1}H-^{13}C correlation was 4 hr, 18 min. All data were processed with Bruker's Topspin 4.0.7. ^{1}H chemical shifts were internally referenced to DSS (0.00 ppm), with the ^{13}C chemical shifts referenced indirectly using the gyromagnetic ratios of ^{13}C/^{1}H (*44*). The ^{19}F chemical shifts were internally referenced to trifluoroacetic acid (-75.51 ppm) (*45*).

Small molecule titration. 5FU hHBV ε was diluted to ~ 0.4 mM in 10 mM Na_3PO_4 (pH 6.5), 0.02 % NaN_3, and 0.1 mM DSS in ~ 150 μL. The small molecule was titrated from a 50 mM stock prepared in d6-DMSO to a maximum concentration of ~ 200 μM. 512 transients were recorded for each complex point with acquisition times of 300 ms in ω_2 and 120 ms in ω_1. Carrier positions and recycling delay are as described above. Reduced experimental time was achieved with a 25% non-uniform sampling (NUS) scheme (*46*). Chemical shift perturbations (CSPs) were calculated as follows (*38*):

Equation 2 $$CSP = \sqrt{(\Delta\delta_{19F})^2 + \left(\frac{\partial_{13C}}{\partial_{19F}}(\Delta\delta_{13C})\right)^2}$$

Where $\partial_{13C/19F}$ corresponds to the range in chemical shifts for the ^{13}C/^{19}F dimensions and $\Delta\delta_{13C/19F}$ for the change in ^{13}C/^{19}F chemical shift upon addition of small molecule.

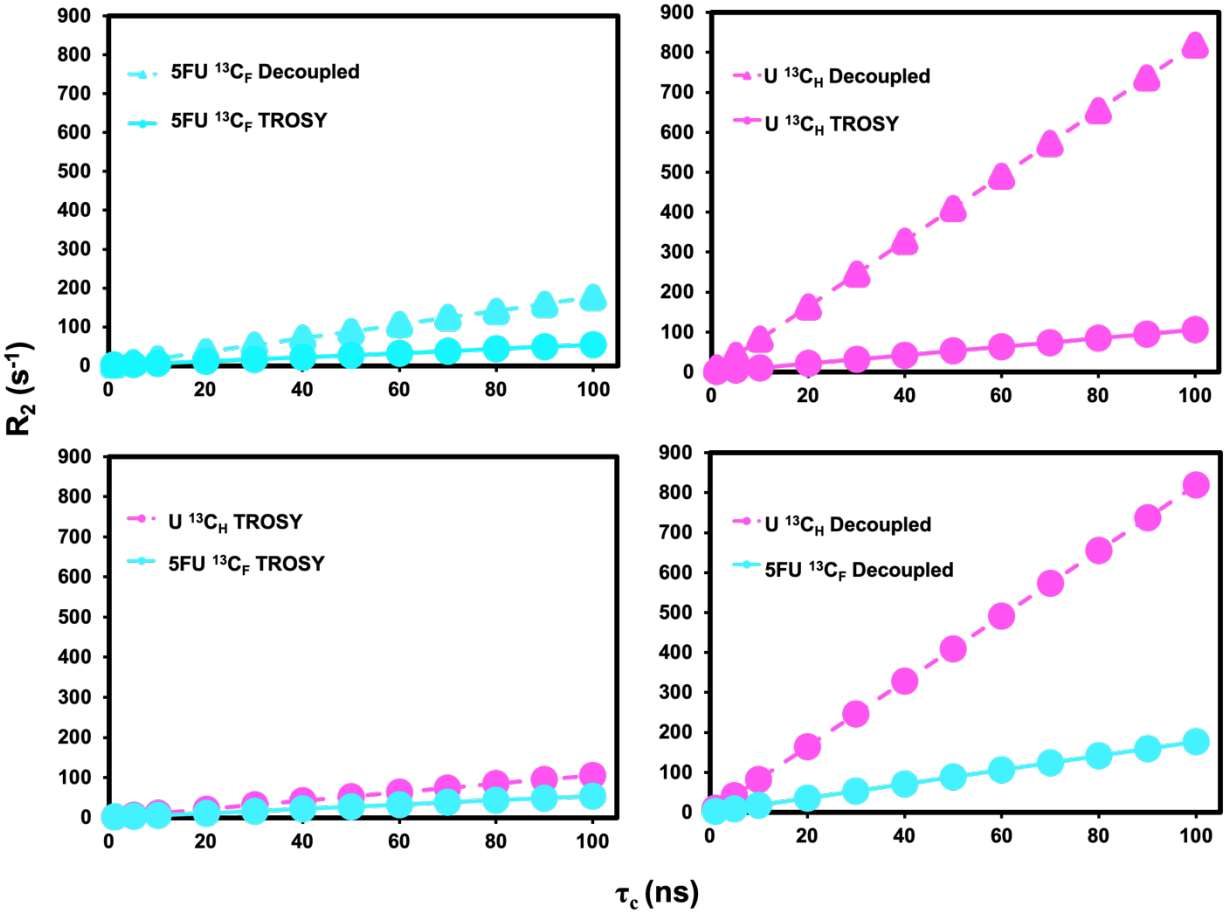

Figure S1. Theoretical R_2 values for the $^{13}C_F$ and $^{13}C_H$ components as a function of τ_c. Theoretical R_2 values are taken at the commercially available magnetic field strength closest to the maximum TROSY effect ($^{13}C_H$ = 950 MHz; $^{13}C_F$ = 600 MHz) and 25 °C.

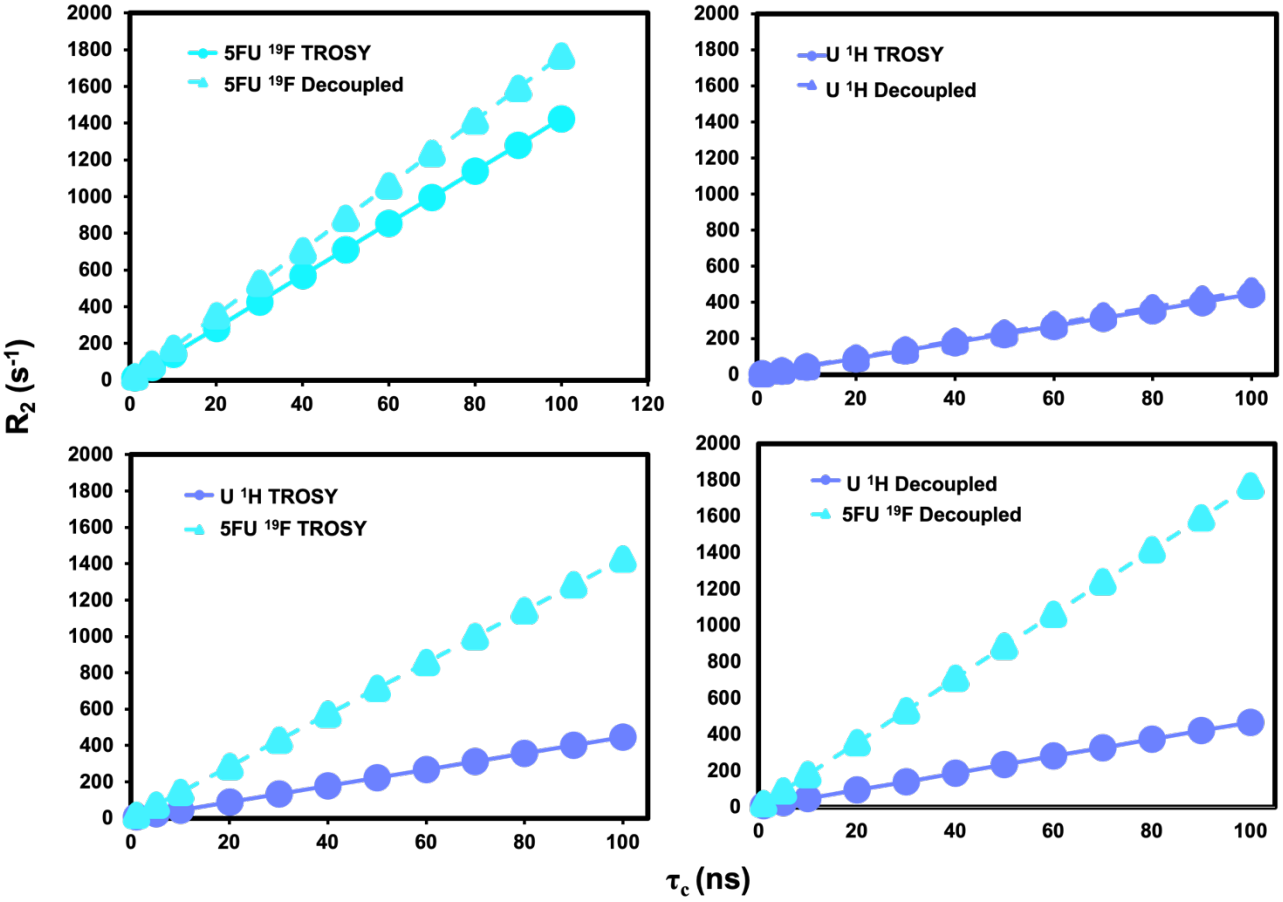

Figure S2. Theoretical R_2 values for the $^{19}F_C$ and $^{1}H_C$ components as a function of τ_c. Theoretical R_2 values are taken at the commercially available magnetic field strength closest to the maximum TROSY effect ($^{13}C_H$ = 950 MHz; $^{13}C_F$ = 600 MHz) and 25 °C.

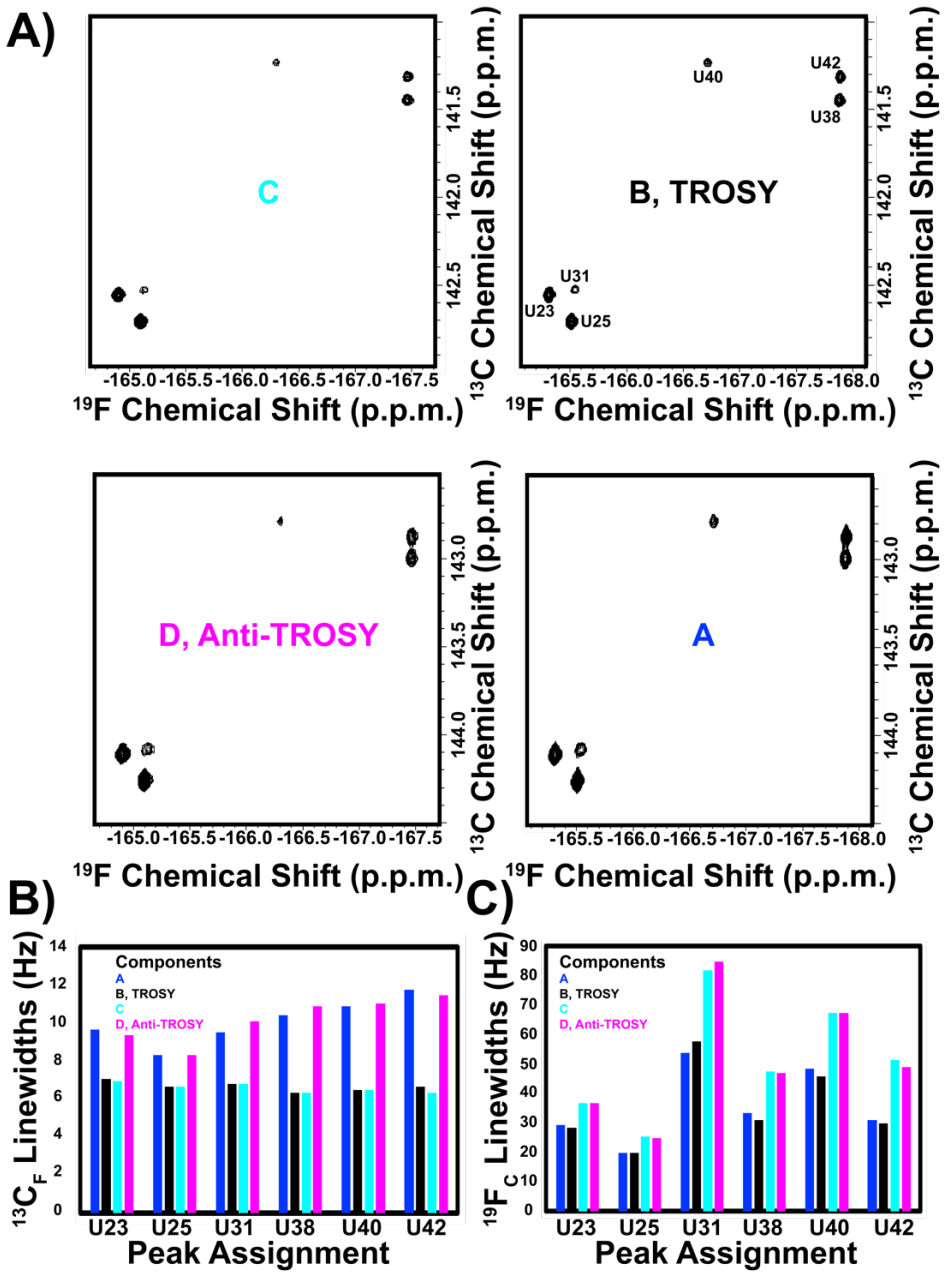

Figure S3. 5FU TAR-2 four components of the ^{19}F-^{13}C correlation. (A) Spectra of A, bottom right, B, TROSY, top right, C, top left, and D, anti-TROSY, bottom left, components of the ^{19}F-^{13}C correlations of 5FU TAR-2. All contours are set identically in all four spectra. Peak assignments are indicated on the B, TROSY spectrum. In all four spectra, the carrier was set to -167.0 and 140.0 ppm for ^{19}F (ω_2) and ^{13}C (ω_1), respectively. 32 transients were collected for each complex point with acquisitions times of 302 ms for ω_2 and 132 ms for ω_1. An interscan delay of 2.0 s was used. Quantification of **(B)** ^{13}C and **(C)** ^{19}F linewidths for each of the four components.

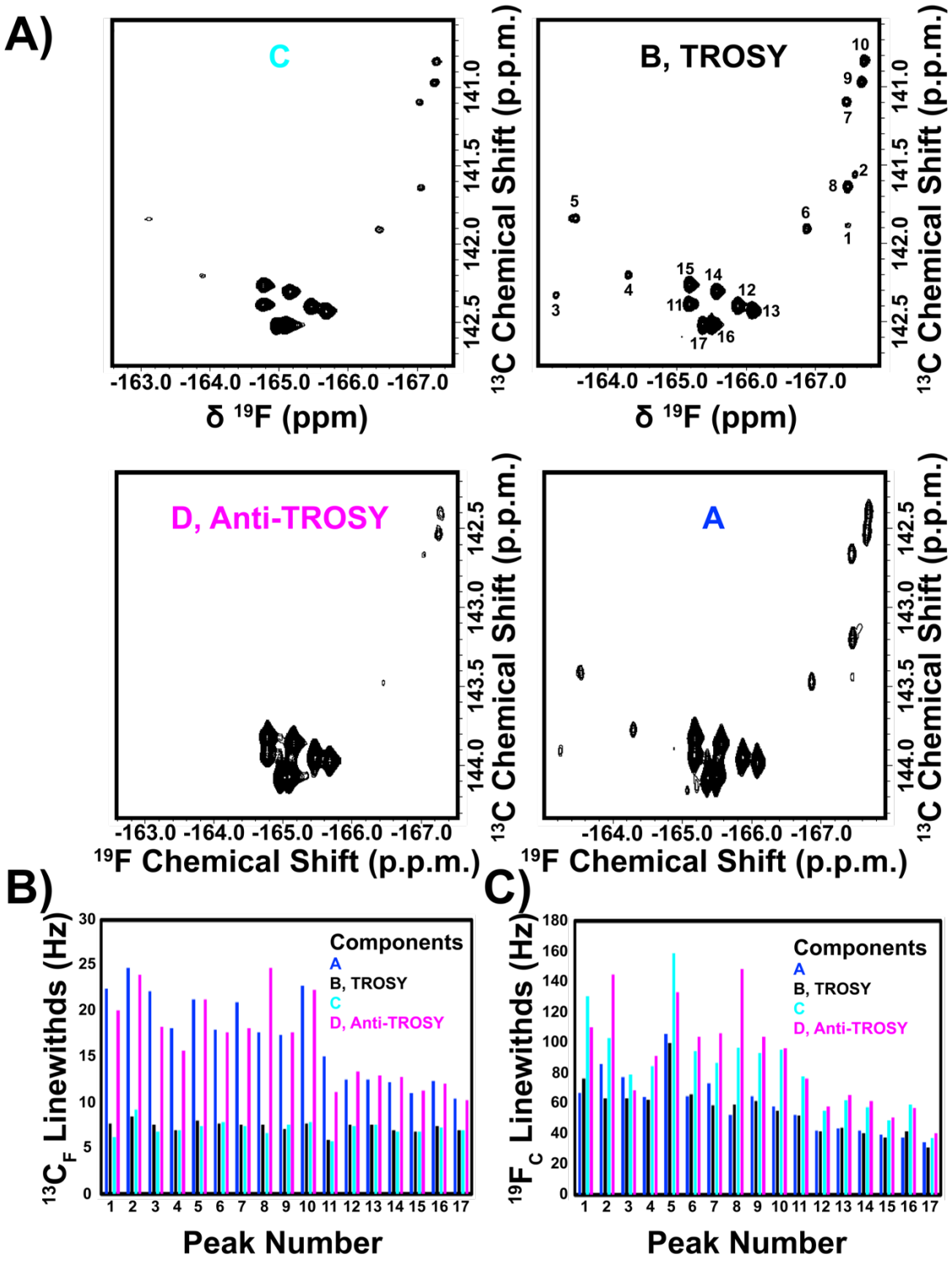

Figure S4. 5FU hHBV ε four components of the ^{19}F-^{13}C correlation. (A) Spectra of A, bottom right, B, TROSY, top right, C, top left, and D, anti-TROSY, bottom left, components of the ^{19}F-^{13}C correlations of 5FU hHBV . All contours are set identically in the four spectra. Peak assignments are indicated on the B, TROSY spectrum. In all four spectra, the carrier was set to -167.0 and 140.0 ppm for ^{19}F (ω_2) and ^{13}C (ω_1), respectively. 32 transients were collected for each complex point with acquisitions times of 302 ms for ω_2 and 132 ms for ω_1. An interscan delay of 2.0 s was used. Quantification of **(B)** ^{13}C and **(C)** ^{19}F linewidths for each of the four components.

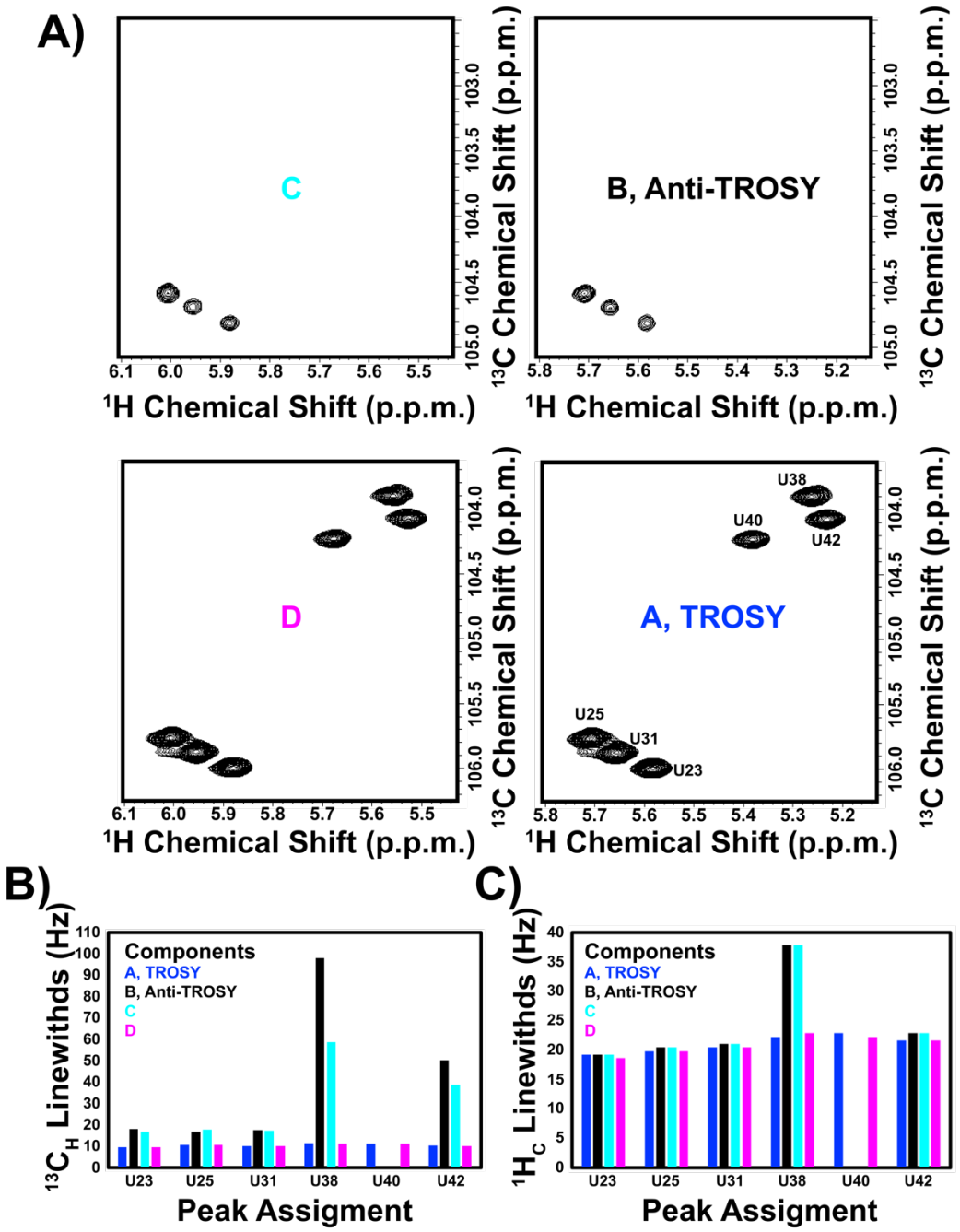

Figure S5. WT TAR-2 four components of the ^{1}H-^{13}C correlation. (A) Spectra of A, TROSY, bottom right, B, Anti-TROSY, top right, C, top left, and D, bottom left, components of the ^{19}H-^{13}C correlations of WT TAR-2. All contours are set identically in all four spectra. Peak assignments are indicated on the A, TROSY spectrum. In all four spectra, the carrier was set to 4.7 ppm and 100.5 ppm for ^{1}H (ω_2) and ^{13}C (ω_1), respectively. 32 transients were collected for each complex point with acquisitions times of 302 ms for ω_2 and 132 ms for ω_1. An interscan delay of 2.0 s was used. Quantification of **(B)** ^{13}C and **(C)** ^{1}H linewidths for each of the four components. Note that U40 was not observed in the B, Anti-TROSY and C spectra.

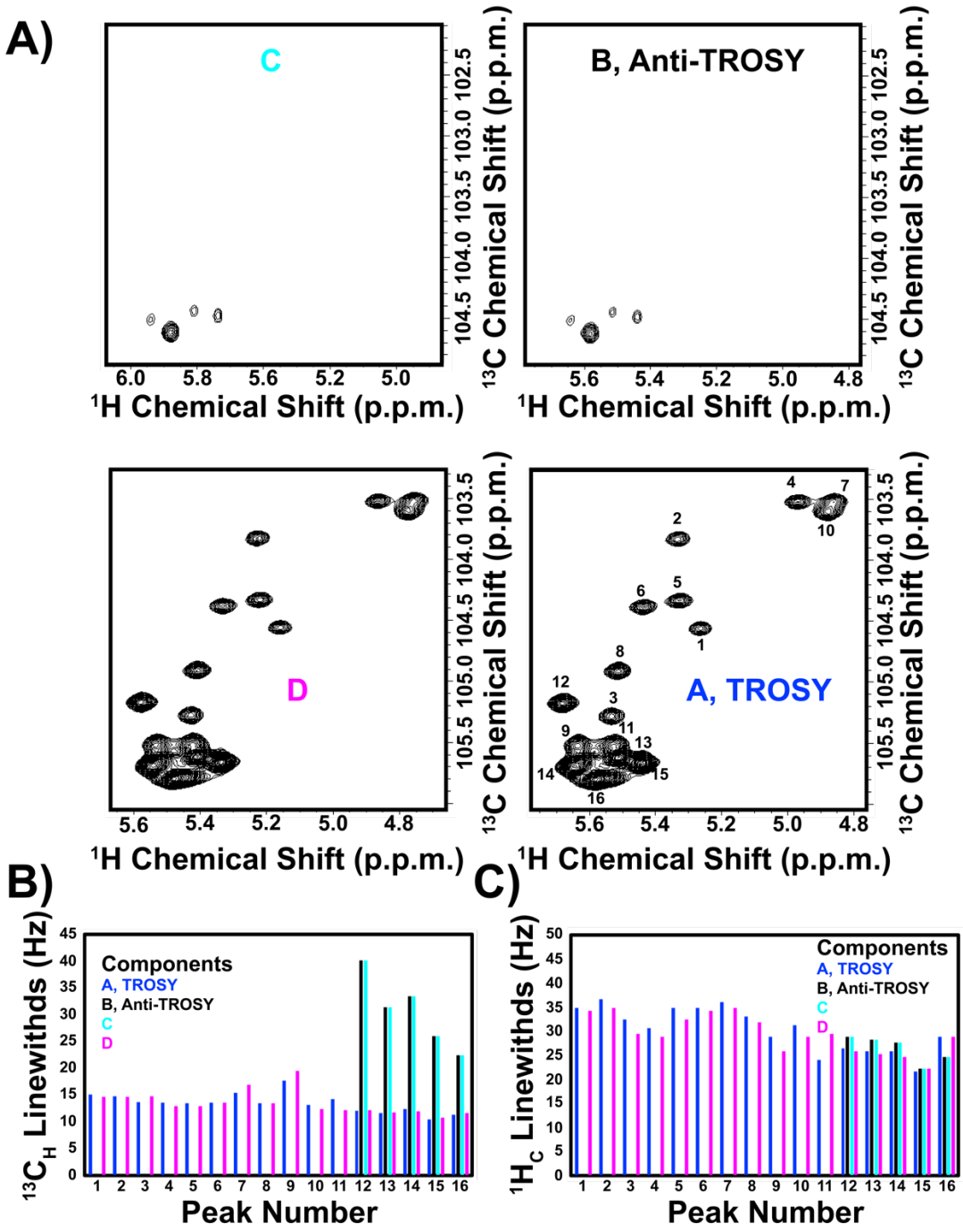

Figure S6. WT hHBV ε four components of the ^{1}H-^{13}C correlation. (A) Spectra of A, TROSY, bottom right, B, Anti-TROSY, top right, C, top left, and D, bottom left, components of the ^{19}H-^{13}C correlations of WT hHBV ε. All contours are set identically in all four spectra. Peak assignments are indicated on the A, TROSY spectrum. In all four spectra, the carrier was set to 4.7 ppm and 100.5 ppm for ^{1}H (ω_2) and ^{13}C (ω_1), respectively. 32 transients were collected for each complex point with acquisitions times of 302 ms for ω_2 and 132 ms for ω_1. An interscan delay of 2.0 s was used. Quantification of **(B)** ^{13}C and **(C)** ^{1}H linewidths for each of the four components. Note that only peaks 12, 13, 14, 15, and 16 were observed in the B, anti-TROSY, and C spectra.

Table S1. Thermodynamic parameters for WT and 5FU RNAs.

	WT HIV-2 TAR	5FU HIV-2 TAR	WT hHBV ε	5FU hHBV ε
ΔH / kcalmol^{-1}	-91 ± 6	-101 ± 6	-130. ± 5	-117 ± 6
ΔS / kcalmol^{-1}K^{-1}	-0.26 ± 0.02	-0.28 ± 0.02	-0.40 ± 0.01	-0.36 ± 0.01
T_m /K	355.6 ± 0.5	357.4 ± 0.4	327.0 ± 0.1	327.1 ± 0.1

Table S2. Results for 1-methyl uracil, ^{13}C5

Method	*basis set*	δ_{11}	δ_{22}	δ_{33}	ϕ	Δ	σ_{iso}	σ_{ref}	δ_{iso}
Hartree-Fock	pcSseg-2	91.5	-17.4	-74.1	17.5	-137	87.9		
M06	pcSseg-2	91.9	-8.3	-83.6	14.2	-138	61.3	176.2	114.9
PBE0	pcSseg-2	85.8	-9.0	-76.8	12.5	-129	74.2	186.5	112.3
PBE0	pcSseg-3	85.8	-8.9	-76.9	12.4	-129			
B3LYP	pcSseg-2	85.9	-10.0	-75.9	12.1	-129	69.0	181.7	112.7
PBE	pcSseg-2	83.2	-8.5	-74.7	10.6	-125	69.5	181.8	112.3
OLYP	pcSseg-2	80.8	-9.3	-71.5	10.7	-121	73.8	182.6	108.8
OLYP	pcSseg-3	80.5	-9.4	-71.1	10.7	-121			
MP2	pcSseg-2	81.1	-11.6	-69.5	11.2	-122	88.6		
Stikoff/Case	iii-iglo	80	-8	-73	10.7	-121			
ssNMR uracil		81.4	-3.1	-78.4		-122			99.6

Principal components δ of the traceless chemical shift tensor, in ppm; ϕ is the angle between δ_{11} and the C-H bond; Δ is $(\delta_{22}+\delta_{33})/2 - \delta_{11}$. σ_{ref} is the result for TMS, and δ_{iso} is $\sigma_{ref} - \sigma_{iso}$.

Table S3. Results for 1-methyl,5-fluoro-uracil, ^{13}C5 and ^{19}F5

			^{13}C5				*^{19}F5*		
Method	*basis set*	δ_{11}	δ_{22}	δ_{33}	Δ	δ_{11}	δ_{22}	δ_{33}	Δ
Hartree-Fock	pcSseg-2	78.4	-20.2	-58.2	-118	39.0	5.7	-44.7	-59
PBE0	pcSseg-2	64.9	-9.4	-55.5	-97	53.9	22.9	-76.7	-81
PBE	pcSseg-2	58.8	-5.9	-52.8	-88	61.2	28.6	-89.8	-92
OLYP	pcSseg-2	56.6	-5.9	-50.8	-85	58.5	25.1	-83.5	-88
MP2	pcSseg-2	59.9	-9.8	-50.1	-90	50.0	14.7	-64.8	-75

Entities are defined as in Table S2.

REFERENCES AND NOTES

1. K. D. Warner, C. E. Hajdin, K. M. Weeks, Principles for targeting RNA with drug-like small molecules. *Nat. Rev. Drug Discov.* **17**, 547–558 (2018).

2. A. Donlic, A. E. Hargrove, Targeting RNA in Mammalian Systems with Small Molecules. *WIREs RNA* **9**, e1477 (2018).

3. L. J. Alvarado, R. M. LeBlanc, A. P. Longhini, S. C. Keane, N. Jain, Z. F. Yildiz, B. S. Tolbert, V. M. D'Souza, M. F. Summers, C. Kreutz, T. K. Dayie, Regio-selective chemical-enzymatic synthesis of pyrimidine nucleotides facilitates RNA structure and dynamics studies. *Chembiochem* **15**, 1573–1577 (2014).

4. A. P. Longhini, R. M. LeBlanc, O. Becette, C. Salguero, C. H. Wunderlich, B. A. Johnson, V. M. D'Souza, C. Kreutz, T. K. Dayie, Chemo-enzymatic synthesis of site-specific isotopically labeled nucleotides for use in NMR resonance assignment, dynamics and structural characterizations. *Nucleic Acids Res.* **44**, e52 (2016).

5 F. Rastinejad, C. Evilia, P. Lu, Studies of nucleic acids and their protein interactions by ^{19}F NMR. *Methods Enzymol.* **261**, 560–575 (1995).

6. M. Hennig, L. G. Scott, E. Sperling, W. Bermel, J. R. Williamson, Synthesis of 5-fluoropyrimidine nucleotides as sensitive NMR probes of RNA structure. *J. Am. Chem. Soc.* **129**, 14911–14921 (2007).

7. J. Horowitz, O. Ching-Nan, M. Ishaq, J. Ofengand, J. Bierbaum, Isolation and partial characterization of Escherichia coli valine transfer RNA with uridine and uridine-derived residues replaced by 5-fluorouridine. *J. Mol. Biol.* **88**, 301–312 (1974).

8. J. Horowitz, J. Ofendgan, W. Daniel Jr., M. Cohn, ^{19}F nuclear magnetic resonance of 5-fluorouridine-substituted $tRNA_1^{Val}$ from Escherichia coli. *J. Biol. Chem.* **252**, 4418–4420 (1977).

9. A. G. Marshall, J. L. Smith, Nuclear Spin-Labeled Nucleic Acids. 1. ^{19}F Nuclear Magnetic Resonance of Escherichia coli 5-Fluorouracil-5S-RNA. *J. Am. Chem. Soc.* **99**, 635–636 (1977).

10. S. L. Cobb, C. D. Murphy, ^{19}F NMR applications in chemical biology. *J. Fluor. Chem.* **130**, 132–143 (2009).

11. F. Guo, Q. Li, C. Zhou, Synthesis and biological applications of fluoro-modified nucleic acids. *Org. Biomol. Chem.* **15**, 9552–9565 (2017).

12. F. Sochor, R. Silvers, D. Müller, C. Richter, B. Fürtig, H. Schwalbe, ^{19}F -labeling of the adenine H2-site to study large RNAs by NMR spectroscopy. *J. Biomol. NMR* **64**, 63–74 (2016).

13. A. Boeszoermenyi, S. Chhabra, A. Dubey, D. L. Radeva, N. T. Burdzhiev, C. D. Chanev, O. I. Petrov, V. M. Gelev, M. Zhang, C. Anklin, H. Kovacs, G. Wagner, I. Kuprov, K. Takeuchi, H. Arthanari, Aromatic ^{19}F-^{13}C TROSY: a background-free approach to probe biomolecular structure, function, and dynamics. *Nat. Methods* **16**, 333–340 (2019).

14. M. Hennig, M. L. Munzarová, W. Bermel, L. G. Scott, V. Sklenář, J. R. Williamson, Measurement of Long-Range ^{1}H–^{19}F Scalar Coupling Constants and Their Glycosidic Torsion Dependence in 5-Fluoropyrimidine-Substituted RNA. *J. Am. Chem. Soc.* **128**, 5851–5858 (2006).

15. T. Knaus, M. Nassal, The encapsidation signal on the hepatitis B virus RNA pregenome forms a stem-loop structure that is critical for its function. *Nucleic Acids Res.* **21**, 3967–3975 (1993).

16. S. Flodell, M. Petersen, F. Girard, J. Zdunek, K. Kidd-Ljunggren, J. Schleucher, S. Wijmenga, Solution structure of the apical stem-loop of the human hepatitis B virus encapsidation signal. *Nucleic Acids Res.* **34**, 4449–4457 (2006).

17. J. Santalucia Jr., L. X. Shen, Z. Cai, H. Lewis, I. Tinoco Jr., Synthesis and NMR of RNA with selective isotopic enrichment in the bases. *Nucleic Acids Res.* **23**, 4913–4921 (1995).

18. C. H. Wunderlich, R. Spitzer, T. Santner, K. Fauster, M. Tollinger, C. Kreutz, Synthesis of (6-C-13)Pyrimidine Nucleotides as Spin-Labels for RNA Dynamics. *J. Am. Chem. Soc.* **134**, 7558–7569 (2012).

19. G. S. Lal, W. Pastore, R. Pesaresi, A Convenient Synthesis of 5-Fluoropyrimidines Using 1-(Chloromethyl)-4-fluoro-1,4-diazabicyclo[2.2.2]octane Bis(tetrafluoroborate)-SELECTFLUOR Reagent. *J. Organomet. Chem.* **60**, 7340–7342 (2005).

20. H. S. Rangwala, J.W. Giraldes, V. J. Gurvich, Synthesis and purification of [2-^{13}C]-5-fluorouracil. *J. Label. Compd. Radiopharm.* **54**, 340–343 (2011).

21. R. J. Cushley, S. R. Lipsky, Reactions of 5-fluorouracil derivatives with sodium deuteroxide. *Tetrahedron Lett.* **52**, 5393–5396 (1968).

22. L. J. Alvarado, A. P. Longhini, R. M. LeBlanc, B. Chen, C. Kreutz, T. K. Dayie, Chemo-enzymatic synthesis of selectively ^{13}C/^{15}N-labeled RNA for NMR structural and dynamics studies. *Methods Enzymol.* **549**, 133–162 (2014).

23. P. C. Bevilacqua, T. S. Brown, S. I. Nakano, R. Yajima, Catalytic Roles for Proton Transfer and Protonation in Ribozymes. *Biopolymers* **73**, 90–109 (2004).

24. L. G. Scott, M. Hennig, ^{19}F-site-specific-labeled nucleotides for nucleic acid structural analysis by NMR. *Methods Enzymol.* **566**, 59–87 (2016).

25. J. L. Mergny, L. Lacroix, UV melting of G-quadruplexes. *Curr. Protoc. Nucleic Acid Chem.* **37**, 17.1.1–17.1.15 (2009).

26. N. C. Handy, A. J. Cohen, Left-right correlation energy. *Mol. Phys.* **99**, 403–412 (2001).

27. C. Adamo, V. Barone, Toward reliable density functional methods without adjustable parameters: The PBE0 model. *J. Chem. Phys.* **110**, 6158–6170 (1999).

28. F. Jensen, Segmented contracted basis sets optimized for nuclear magnetic shielding. *J. Chem. Theory Comput.* **11**, 132–138 (2015).

29. M. J. Frisch, G. W. Trucks, H. B. Schlegel, G. E. Scuseria, M. A. Robb, J. R. Cheeseman, G. Scalmani, V. Barone, G. A. Petersson, H. Nakatsuji, X. Li, M. Caricato, A. V. Marenich, J. Bloino, B. G. Janesko, R. Gomperts, B. Mennucci, H. P. Hratchian, J. V. Ortiz, A. F. Izmaylov, J. L.

Sonnenberg, D. Williams-Young, F. Ding, F. Lipparini, F. Egidi, J. Goings, B. Peng, A. Petrone, T. Henderson, D. Ranasinghe, V. G. Zakrzewski, J. Gao, N. Rega, G. Zheng, W. Liang, M. Hada, M. Ehara, K. Toyota, R. Fukuda, J. Hasegawa, M. Ishida, T. Nakajima, Y. Honda, O. Kitao, H. Nakai, T. Vreven, K. Throssell, J. Montgomery, J. A., J. E. Peralta, F. Ogliaro, M. J. Bearpark, J. J. Heyd, E. N. Brothers, K. N. Kudin, V. N. Staroverov, T. A. Keith, R. Kobayashi, J. Normand, K. Raghavachari, A. P. Rendell, J. C. Burant, S. S. Iyengar, J. Tomasi, M. Cossi, J. M. Millam, M. Klene, C. Adamo, R. Cammi, J. W. Ochterski, R. L. Martin, K. Morokuma, O. Farkas, J. B. Foresman, D. J. Fox, Gaussian 16, Revision A.03 (2016).

30. I. Kuprov, N. Wagner-Rundell, P. J. Hore, Bloch-Redfield-Wangsness theory engine implementation using symbolic processing software. *J. Magn. Reson.* **184**, 196–206 (2007).

31. J. Weigelt, Single scan, sensitivity- and gradient-enhanced TROSY for multidimensional NMR experiments. *J. Am. Chem. Soc.* **120**, 10778–10779 (1998).

32. K. Pervushin, R. Riek, G. Wider, K Wüthrich, Attenuated T_2 relaxation by mutual cancellation of dipole-dipole coupling and chemical shift anisotropy indicates an avenue to NMR structures of very large biological macromolecules in solution. *Proc. Natl. Acad. Sci. U.S.A.* **94**, 12366–12371 (1997).

33. T. Carlomagno, I. Amata, J. R. Williamson, M. Hennig, NMR assignments of HIV-2 TAR RNA. *Biomol. NMR Assign.* **2**, 167–169 (2008).

34. W. Chu, J. Horowitz, ^{19}F NMR of 5-fluorouracil-substituted transfer RNA transcribed in vitro: resonance assignment of fluorouracil-guanine base pairs. *Nucleic Acids Res.* **17**, 7241–7252 (1989).

35. C. Dalvit, A. Vulpetti, Ligand-Based Fluorine NMR Screening: Principles and Applications in Drug Discovery Projects. *J. Med. Chem.* **62**, 2218–2244 (2019).

36. A. Divakaran, S. E. Kirberger, W. C. K. Pomerantz, SAR by (Protein-Observed) ^{19}F NMR. *Acc. Chem. Res.* **52**, 3407–3418 (2019).

37. U. S. Gill, P. T. F. Kennedy, The impact of currently licensed therapies on viral and immune responses in chronic hepatitis B: Considerations for future novel therapeutics. *J. Viral Hepat.* **26**, 4–15 (2019).

38. M. P. Williamson, Using chemical shift perturbation to characterise ligand binding. *Prog. Nucl. Magn. Reson. Spectrosc.* **73**, 1–16 (2013).

39 S. Barton, X. Heng, B. A. Johnson, M. F. Summers, Database proton NMR chemical shifts for RNA signal assignment and validation. *J. Biomol. NMR* **55**, 33–46 (2013).

40. F. H. Crick, Codon--anticodon pairing: the wobble hypothesis. *J. Mol. Biol.* **19**, 548–555 (1966).

41. G. Varani, W. H. McClain, The G x U wobble base pair. A fundamental building block of RNA structure crucial to RNA function in diverse biological systems. *EMBO Rep.* **1**, 18–23 (2000).

42. P. Ananth, G. Goldsmith, N. Yathindra, An innate twist between Crick's wobble and Watson-Crick base pairs. *RNA* **19**, 1038–1053 (2013).

43. P.K. Arthur, L.J. Alvarado, T.K. Dayie, Expression, purification and analysis of the activity of enzymes from the pentose phosphate pathway. *Protein Expr. Purif.* **76**, 229–237 (2011).

44. T. Aeschbacher, M. Schubert, F. H. T. Allain, A procedure to validate and correct the ^{13}C chemical shift calibration of RNA datasets. *J. Biomol. NMR* **52**, 179–190 (2012).

45. C. P. Rosenau, B. J. Jelier, A. D. Gossert, A. Togni, Exposing the Origins of Irreproducibility in Fluorine NMR Spectroscopy. *Angew. Chem. Int. Ed.* **57**, 9528–9533 (2018).

46. D. Rovnyak, D. P. Frueh, M. Sastry, Z. Y. J. Sun, A. S. Stern, J. C. Hoch, G. Wagner, Accelerated acquisition of high resolution triple-resonance spectra using non-uniform sampling and maximum entropy reconstruction. *J. Magn. Reson.* **170**, 15–21 (2004).